Nuclear Engineering and Design 428 (2024) 113487

Contents lists available at ScienceDirect

Nuclear Engineering and Design

journal homepage: www.elsevier.com/locate/nucengdes

POD–ANN as digital twins for surge line thermal stratification

Ying Yang [a], Xielin Zhao [b], Qian Cheng [b], Ruiwen Guo [b], Meie Li [a,*], Jinxiong Zhou [b]

[a] State Key Laboratory for Mechanical Behavior of Materials, School of Materials Science and Engineering, Xi'an Jiaotong University, Xi'an 710049, People's Republic of China

[b] State Key Laboratory for Strength and Vibration of Mechanical Structures, School of Aerospace, Xi'an Jiaotong University, Xi'an 710049, People's Republic of China

ARTICLE INFO

Dataset link: https://github.com/XJTU-Zhou-group/Digital Twin

Keywords:
Thermal stratification
Surge line
Proper orthogonal decomposition (POD)
Artificial neural network (ANN)
Digital twin

ABSTRACT

This paper describes a hybrid proper orthogonal decomposition (POD) and artificial neural network (ANN) strategy to construct digital twins of a pressurizer surge line under thermal stratification conditions. The one-way coupled conjugate heat transfer and thermal stress analysis was conducted by use of parametric modeling and the introduction of the inverse distance weighted interpolation for the grid mapping, which allows for the mapped grids to have the same number of nodes regardless of variations of surge line geometries. A snapshot-based POD was utilized to obtain truncated lower-order modes and the full-order system response was projected onto these modes with reduced state coefficients. Then the ANN was employed to establish a surrogate model between the five chosen design variables of interest and the reduced state coefficients, resulting in a surrogate-assisted digital twin for a pressurizer surge line. Prediction of fluid–structure interface temperature and thermal stress distribution was thus achieved in an in-line real-time manner for a wide range of parameter variations. We publicly share all code implementations, and we believe that our efforts open a door for the digital twining of thermo–fluid–structure interaction problems

1. Introduction

The phenomenon of thermal stratification of cold and hot water may occur in horizontal pipelines at low flow velocities (Talja and Hansjosten, 1990; Miksch et al., 1985; Kim et al., 1993; Liu and Cranford, 1991). The cold water is heavier than the hot water and flows through the pipe beneath the hot water, resulting in circumferentially varying temperatures of the pipe cross-section, which is called thermal stratification. Due to the different velocities of the two fluid layers, the temperature in the interface is not constant, but fluctuating. When the temperature in the mixing interface fluctuates rapidly, the so-called thermal striping occurs. Thermal stratification and thermal striping may occur in piping systems in nuclear power plants such as the pressurizer surge lines, emergency core cooling injection lines, residual heat removal lines, feedwater lines, and others where hot and cold fluids may come in contact with each other (Kim et al., 1993). As a result of the thermal stratification in the piping system, the unintended thermal restriction due to supports can potentially cause plastic deformation, a high level of local stress, low-cycle fatigue, and functional impairment of the pipeline (Liu and Cranford, 1991).

Among various pipes in nuclear power plants, the pressurizer surge lines have been identified to be more susceptible to thermal stratification and several incidents have been reported that raised significant safety concerns. The surge line is a curved pipe connecting the pressurizer containing relatively hot water and the hot leg of the reactor coolant system (RCS) filled with relatively cold water. A pressurizer is a pressure vessel used to maintain the pressure in the primary loop of the pressurized water reactor (PWR) plant. The PWR plant undergoes load changes that depend on the electrical demand on the power grid and are stochastic. The electrical load changes cause the fluctuation of coolant temperature and pressure. To maintain a constant pressure, the coolant flows either from the pressurizer to the hot leg of the RCS through the surge line or vice versa. If the letdown flow from the pressurizer to the hot leg is greater than the charging flow from the hot leg to the pressurizer, an outsurge occurs resulting in a pressurizer level decrease. In contrast, an insurge happens if the charging flow is greater than the letdown flow and the pressurizer level increases. Talja and Hansjosten (1990) reported results of thermal stratification tests in a horizontal pipeline at the HDR-facility. The transient local stress due to the temperature fluctuations in the mixing layer has been evaluated. They also estimated the fatigue of piping due to local stress fluctuations. Liu and Cranford (1991) presented a method to evaluate the thermal stress ranges under thermal stratification loadings. The thermal cycling associated with operating transients in the surge line was also discussed. Kim et al. (1993) performed an evaluation of thermal

* Correspondence to: 28 Xianning West Road, Beilin District, Xi'an City, Shaanxi Province, People's Republic of China.
E-mail address: limeie@mail.xjtu.edu.cn (M. Li).

https://doi.org/10.1016/j.nucengdes.2024.113487
Received 16 December 2023; Received in revised form 2 July 2024; Accepted 18 July 2024
Available online 26 July 2024

stratification test data from the HDR test series and obtained a thermal loading spectrum as a function of flow velocity. They then applied the spectrum for thermal fatigue evaluation of typical pressurizer surge lines. Yu et al. (1997) investigated the deformation, and temperature in the surge lines of the YGN (Young Gwang Nuclear Power Plant) units 3 and 4 in Korea. A thermal–hydraulic model for stratified flow, as well as a finite element method (FEM) for stress analysis, were presented. Do Kweon et al. (2008) performed a parametric study on peak temperature and peak stress intensity of pipe cross sections due to thermal stratification, and a modified equation was proposed to determine the peak stress intensity range, serving as a supplement to the ASME B&PV Code, Section 3, subsection NB-3600. Kang et al. (2011) carried out a conjugate heat transfer analysis for a pressurizer surge line subjected to thermal stratification. Transient temperature distributions in the wall of the surge line were calculated under either outsurge or insurge conditions, and the thermal load from CFD simulations was transferred to the FEM code to calculate thermal stress. Due to the importance of structure integrity the thermal stratification in the surge line has been investigated by many researchers (Kim et al., 2005; Qiao et al., 2014; Cai et al., 2017; Jo and Kang, 2010; Kang et al., 2011; Wang et al., 2019; Kim et al., 2013; Yu et al., 2022). Kim et al. (2005) performed a series of experiments to study the thermal stratification in a 1/10 scaled experimental model using the Richard number as the similarity criterion number. Qiao et al. (2014) and Cai et al. (2017) built a 1/3 scaled experimental facility to conduct an experimental study on thermal stratification. The Computational Fluid Dynamics (CFD) method has also been widely used to study the thermal stratification phenomenon in the surge line. Jo and Kang (2010) performed 2D and simplified 3D conjugate heat transfer calculations neglecting the pipe wall thickness to obtain the temperature distribution and stress distribution. Kang et al. (2011) performed realistic three-dimensional transient CFD calculations involving conjugate heat transfer and thermal stress analysis. Tian et al. (2017) conducted experiments on flooding in the surge line of an AP1000 reactor using air water as the working fluid and analyzed the thermal stratification during the process. Wang et al. (2019) built a numerical model of the AP1000 pressurizer surge line to study the thermal stratification characteristics. Muhammad et al. (2022) evaluated the transient thermal distribution and fatigue damage resulting from thermal stratification in the surge line of AP1000 pressurizer systems through CFD analysis employing the Large Eddy Simulation (LES) approach.

Besides the above-mentioned studies of pressurizer surge lines, attention has also been paid to thermal stratification in mixing trees. Hu and Kazimi (2006) carried out benchmark studies of high cycle temperature fluctuations induced by thermal striping in a mixing tree using the LES models. The simulated normalized average temperature and normalized fluctuating temperatures were in good agreement with the measurements. Lee et al. (2009) investigated the temperature fluctuations and structural response of a mixing tree. The study revealed that the temperature difference between the hot and cold fluids of a tree junction and the enhanced heat transfer coefficient due to turbulent mixing are the dominant factors of thermal fatigue of a tree junction. Kamaya and Nakamura (2011) performed a thermal–mechanical coupling simulation to analyze thermal stress and fatigue damage at a mixing tree using ANSYS CFX and Abaqus. The study suggested that, for a precise assessment of the fatigue damage at a mixing tree, the effect of multi-axial stress on the fatigue life together with the mean stress effect should be taken into account. Kamaya (2014) studied the thermal fatigue damage caused by thermal striping at a mixing tree and by thermal stratification at an elbow pipe branched from the main pipe. Emphasis was put on the characteristics of constraint, stress, and crack growth under thermal stress.

The analysis of thermal stratification of piping systems has been tackled either by analytical formulations in the early stage of study or later by coupled fluid–structure simulations. Analytical approaches are efficient but limited by simple geometries and boundary conditions; while high-fidelity simulations are expensive and extremely time-consuming. A number of geometric, physical, and mechanical have been identified as factors that influence thermal stratification and thermal stress. It is desperately needed to perform a systematic parametric study on the effects of various dominant parameters on thermal stratification, giving a design map or parametric sensitivity analysis under all possible combinations of geometric designs and operation conditions. Attaining this goal by exclusive use of high-fidelity simulation is prohibitive due to the exorbitant cost of fluid–structure interaction simulation. Recourse is thus made to develop various surrogate models, which establish a mapping between design variables and responses with a simple explicit function or a black-box function, resulting in the technology called surrogate-assisted digital twins.

A digital twin is a term that is being used for a wide range of things across a wide range of applications, ranging from manufacturing, smart cities, healthcare, and oil refinery management, to aerospace and defense products development (Jones et al., 2020; Tao and Qi, 2019; Fuller et al., 2020; Kritzinger et al., 2018; Wright and Davidson, 2020; Grieves, 2005; Tao et al., 2018). In short, digital twins are real-time, virtual replicas of physical entities. Digital twins can use any sort of model that is a sufficiently accurate representation of the physical object that is being twinned (Wright and Davidson, 2020). One common approach used is to construct a surrogate model or metamodel based on high-fidelity physics-based simulations. A surrogate model is a simplified model, typically data-driven, that runs more quickly than a physics-based model and so can be used to generate updated parameter estimates more quickly.

This surrogate-assisted digital twin can be realized through various approaches, and one approach of particular interest is the hybrid reduced-order modeling (ROM) and deep learning (DL) approach. One of the most popular ROM methods for low-order approximation of high-dimensional problems is the proper orthogonal decomposition (POD) technique (Zhao et al., 2021, 2023; Liu et al., 2024). First proposed in 1901 by Pearson (1901), the POD technique has since been developed and provides an efficient approach for ROM analysis in various applications. Recently, the neural network surrogate model has also attracted great attention from a large number of scholars. This ROM-DL hybrid approach has been applied to a spectrum of computational fluid/structural mechanics problems. San et al. (2019) developed a POD–ANN framework for transient flow simulation. Pawar et al. (2019) proposed a POD-DNN (deep neural network) framework for non-intrusive model reduction of complex fluid flows. Fresca and Manzoni (2022) proposed a POD-DL strategy for nonlinear parameterized PDEs. Regarding the structural and thermal analysis, Im et al. (2021) described a combined Long short-term memory (LSTM) and POD for surrogate modeling of large-scale elasto-plasticity problems; Shah et al. (2022) presented a POD–ANN strategy for one-way coupled steady-state linear thermo–mechanical problems; Park et al. (2013) proposed to perform aircraft structural optimization design using POD–ANN; Eftekhar Azam et al. (2019) presented a hybrid POD–ANN for damage detection in structural systems; He et al. (2022) proposed a reduced-order model based on POD and Back Propagation Neural Network (BPNN) to rapidly estimate the void fraction and temperature field of steam generators. Extension of the hybrid approach to fluid–structure interaction and thermal fluid–structural problems is, however, challenging due partially to the multiphysics complexity of the problems where multiple solvers are involved, and also partially, due to the need for remeshing or dynamic meshing and the mismatch of meshing caused by large geometric variations. Baiges et al. (2020) proposed a finite element reduced-order model based on adaptive mesh refinement and ANN and applied it to a fluid–structure interaction problem. Narrowing down the studies to one-way coupled conjugate heat transfer problems, the development of reduced order modeling and the hybrid approach is still in its infancy and the related works are extremely limited. Blanc et al. (2016) described the application of POD in the

simulation of conjugate heat transfer processes, but limited to the use of only POD techniques.

Here, we describe the hybrid approach by combining POD with ANN for transient conjugate heat transfer in a PWR pressurizer surge line. We use a data-driven snapshot-based method to extract lower-order modes of the fluid field, and the full field response is projected onto these modes to attain POD-reduced state coefficients. The CFD simulations and the structural analysis were carried out through parametric modeling, considering geometric parameters and physical parameter variations in operation. A mapping between input parameters and reduced state coefficients of POD is constructed via ANN, enabling response interpolation and prediction. The hybrid approach brings forward a digital twin for the thermal stratification of surge lines. An issue worth mentioning for this snapshot-based ROM is that there must exist a fixed meshing to generate snapshots even when surge line geometries change. This issue was solved by introducing an inverse distance weighted interpolation scheme. The parametric modeling, fluid and structural simulation, and the digital-twinning are all implemented in commercial software Fluent and ANSYS. We publicly share all codes via the link. We hope that the availability of this hybrid method and its implementation in commercial software will facilitate a wide application in the community and also facilitate interaction between academia and industry.

The paper is organized as follows: The simulation methods for thermal–hydraulic modeling and thermal stress analysis of the surge line are described in Section 2. Section 3 outlines the computational procedure of parametric modeling for conjugate heat transfer in a pressurizer surge line. Section 4.1 introduces the use of background grids and the inverse distance weighting (IDW) method to establish snapshots of variable geometry surge lines. The theory of POD, ANN, and the hybrid POD–ANN approach are expounded in Sections 4.2, 4.3, and 4.4, respectively. The prediction results are compared and discussed in Section 5. Finally, some concluding remarks are given in Section 6.

2. Thermal–hydraulic modeling and stress analysis of surge line

The geometry and locations of monitoring points at specific cross-sections of the pressurizer surge line are illustrated in Fig. 1. This study incorporates five factors: the inner diameter D, the wall thickness δ, and the inclination angle θ of the horizontal part of the surge line, as well as the inlet velocity u and the temperature difference ΔT between the cold water from the hot leg and the hot water from the pressurizer. The arrangement of the tilted horizontal part is shown in Fig. 1(d). The fluid control equations a outlined in Section 2.1, while the independence tests of time step and mesh grids are discussed in Section 2.2. Additionally, the thermal–fluid–solid coupling simulation is introduced in Section 2.3.

2.1. Governing equations

The Reynolds-averaged Navier–Stokes equations for the conservation of mass, momentum, energy, and turbulent quantities for the conjugate heat transfer problem of the surge lines can be expressed as follows:

Mass Conservation Equation:

$$\frac{\partial\left(\rho u_i\right)}{\partial x_i}=0 \tag{1}$$

Momentum Conservation Equation:

$$\frac{\partial\left(\rho u_i\right)}{\partial t}+\frac{\partial}{\partial x_i}\left(\rho u_i u_j\right)=-\frac{\partial p}{\partial x_i}+\frac{\partial}{\partial x_j}\left[\mu\frac{\partial u_i}{\partial x_j}-\rho\overline{u'_i u'_j}\right]+\rho g \tag{2}$$

Energy Conservation equation:

$$\frac{\partial}{\partial x_i}\left(\rho u_i T\right)=\frac{\partial}{\partial x_i}\left[\left(\frac{\lambda}{c_p}+\frac{\mu_t}{\mathrm{Pr}_t}\right)\frac{\partial T}{\partial x_i}\right] \tag{3}$$

$$\mathrm{Pr}_t=\frac{\mu_t c_p}{\lambda_t} \tag{4}$$

where x_i and x_j represent the Cartesian coordinates corresponding to the x, y, and z directions, respectively; u_i is the average velocity; p is the pressure; μ is the dynamic viscosity, representing the fluid's resistance to shear deformation. g_i is the acceleration of gravity along i direction; T is the temperature; λ represents the thermal conductivity of the fluid; c_p is the specific heat; Pr_t is the turbulent Prandtl number, which characterizes the turbulent transport of heat in the fluid. The SST $k-\omega$ turbulence model was adopted in the present study, and the corresponding equations are as follows:

$$\frac{\partial\left(\rho k\right)}{\partial t}+\frac{\partial\left(\rho u_i k\right)}{\partial x_i}=\frac{\partial}{\partial x_i}\left[\left(\mu+\sigma_k u_t\right)\frac{\partial k}{\partial x_i}\right]+G_k-Y_k+S_k \tag{5}$$

$$\frac{\partial\left(\rho\omega\right)}{\partial t}+\frac{\partial\left(\rho u_i\omega\right)}{\partial x_i}=\frac{\partial}{\partial x_j}\left[\Gamma_\omega\frac{\partial\omega}{\partial x_j}\right]+G_\omega-Y_\omega+D_\omega+S_\omega \tag{6}$$

where u_i is the velocity along the x, y, z directions; ω the specific turbulent dissipation rate; G_k is the turbulence kinetic energy; Γ_ω is the diffusion rate of ω. Y_k and Y_ω are the turbulences produced by diffusion.

2.2. Sensitivity tests of the CFD calculation parameters

Time step independency test: In order to evaluate the effect of the time step on the calculation results, a sensitivity analysis was performed for five different physical time steps of 0.3 s, 0.2 s, 0.1 s, 0.15 s and 0.05 s with a fixed number of nodes of about 390,000. Fig. 2(a) shows the results of the root mean square (RMS) temperature calculation for point 1 and point 3 in the cross-section A of the pressurizer surge line for five time steps, points 1 and 3 are illustrated in Fig. 1(b). As shown in Fig. 2(a), the temperature does not change much from 0.15 s to 0.05 s, so the optimal time step for the calculation is chosen to be 0.1 s.

Mesh independency test: To examine the influence of grid refinement on the calculation outcomes, a sensitivity analysis was carried out using four different node numbers ranging from 230,000 to 600,000, maintaining a constant time step of 0.1 s. The results of the RMS temperature calculations for the positions of point 1 and point 3 on the cross-section A of the pressurizer surge line are presented in Fig. 2(b). As depicted in Fig. 2(b), the temperature exhibits minimal variation as the number of nodes increases from 390,000 to 600,000. Consequently, the optimal number of nodes was determined to be 390,000.

2.3. Thermal–fluid–solid coupling analysis

To explore the thermal–hydraulic characteristics of the pressurizer surge line, a conjugate heat transfer analysis is crucial. This analysis encompasses conduction heat transfer in the pipe wall, conductive heat transfer in the water, and the interaction between the pipe and the fluid. The commercial CFD software FLUENT is utilized to simulate transient heat transfer and fluid flow in the surge line. The mathematical models include the mass conservation equation, momentum conservation equation, energy conservation equation, and turbulent equations. The shear stress transport(SST) k-ω turbulent model is adopted which is known to enable high accuracy boundary layer simulation. We adopt the 3-D, double-precision, pressure-based implicit solver, turn on the full buoyancy model, and use the second-order upwind method to discretize the convection terms. The fluid region grid comprises 315,216 elements, while the structural region grid consists of 76,416 elements.

After conducting the thermal–hydraulic analysis, the obtained transient temperature distributions of the surge line are imported into the ANSYS static structural module to calculate thermal stresses and deflections. The thermoelastic analysis based on the finite element method is also conducted with the structural region grid consisting of 76,416 elements. The inlet (connected to the pressurizer) and outlet

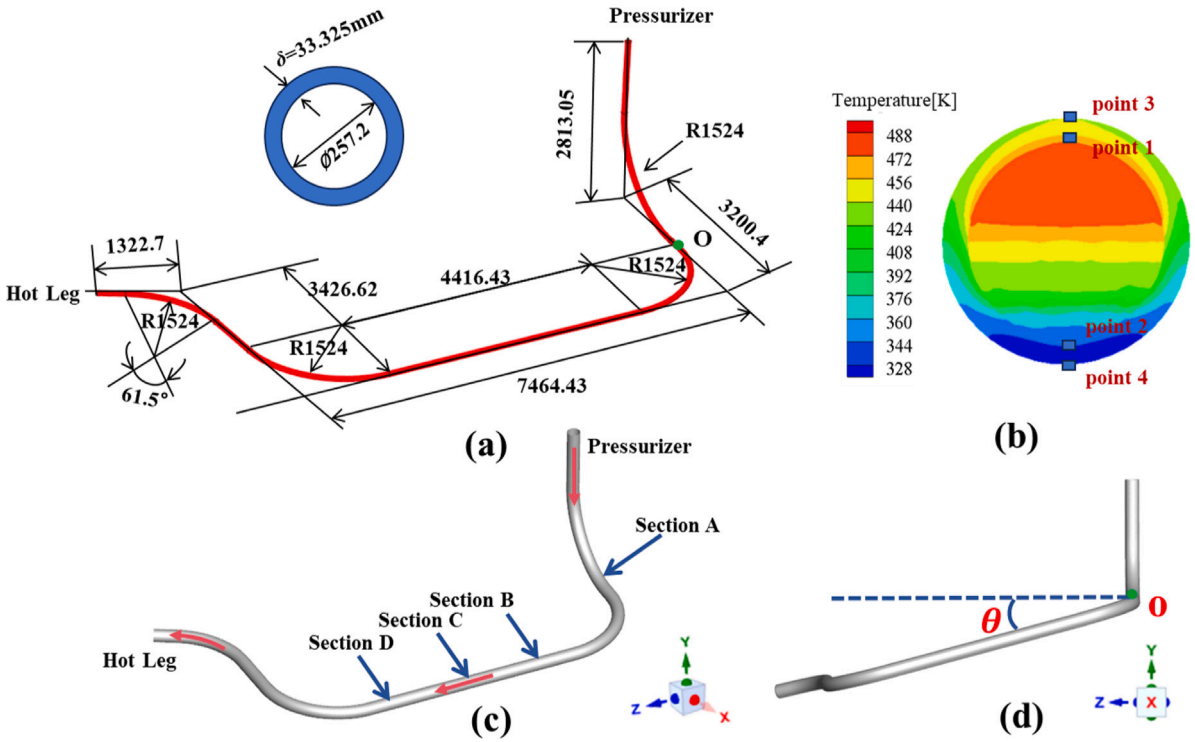

Fig. 1. Problem description of the outsurge and thermal stratification in a PWR pressurizer surge line. (a) Geometric dimensions of a fraction of a pressurizer surge line. (b) Cross sectional temperature distribution of a surge line during thermal stratification. Points for monitoring temperature differences are marked. (c) The pressurizer outsurge flow direction (red arrow) in a surge line and the selected cross sections are used for detecting thermal stratification. (d) Illustration of the tilt angle of the horizontal pipe.

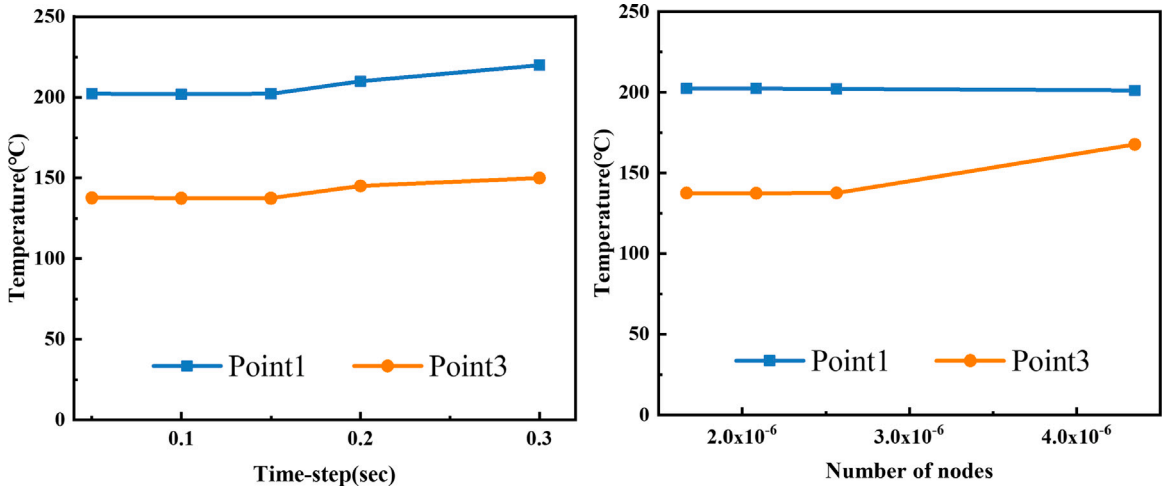

Fig. 2. Cross-section A Pipe internal surface temperature versus time step and number of nodes.

(linked with hot-leg) ends are fixed constraints for the thermoelastic analysis

The model used in this work is validated by comparing it with the research from Kang et al. (2011). In the validation case, the surge line is initially filled with cold water at 324.5 K. At a specific moment, hot water at 491.45 K from the pressurizer is introduced into the upper nozzle of the surge line, which is vertically connected to the pressurizer, with a velocity of 0.07 m/s. The reference pressure is set at 2.2408 MPa. Since power plants typically include an insulation layer around the tube to prevent heat loss, the adiabatic condition is applied to the outer wall surface of the surge line. The physical and mechanical properties of the pipe material used in the analysis are detailed in Table 1. For the thermophysical properties of the coolant, water, refer to Jo and Kang (2010).

Fig. 3(a) presents the transient evolution of the temperature difference between points 1 and 2 on the top and bottom inner wall surfaces at cross-section A. In Fig. 3(b), the temperature difference between points 3 and 4 on the top and bottom outer wall surfaces is displayed. Additionally, Fig. 3(c) and (d) illustrate the transient evolution of the maximum equivalent stress and the maximum deflection, respectively. The obtained results correspond well with Kang's previous research (Kang et al., 2011), supporting the validity of the current model. In Fig. 4(a), the temperature distribution of the surge line and four monitoring sections at the 300 s mark is depicted, while Fig. 4(b)

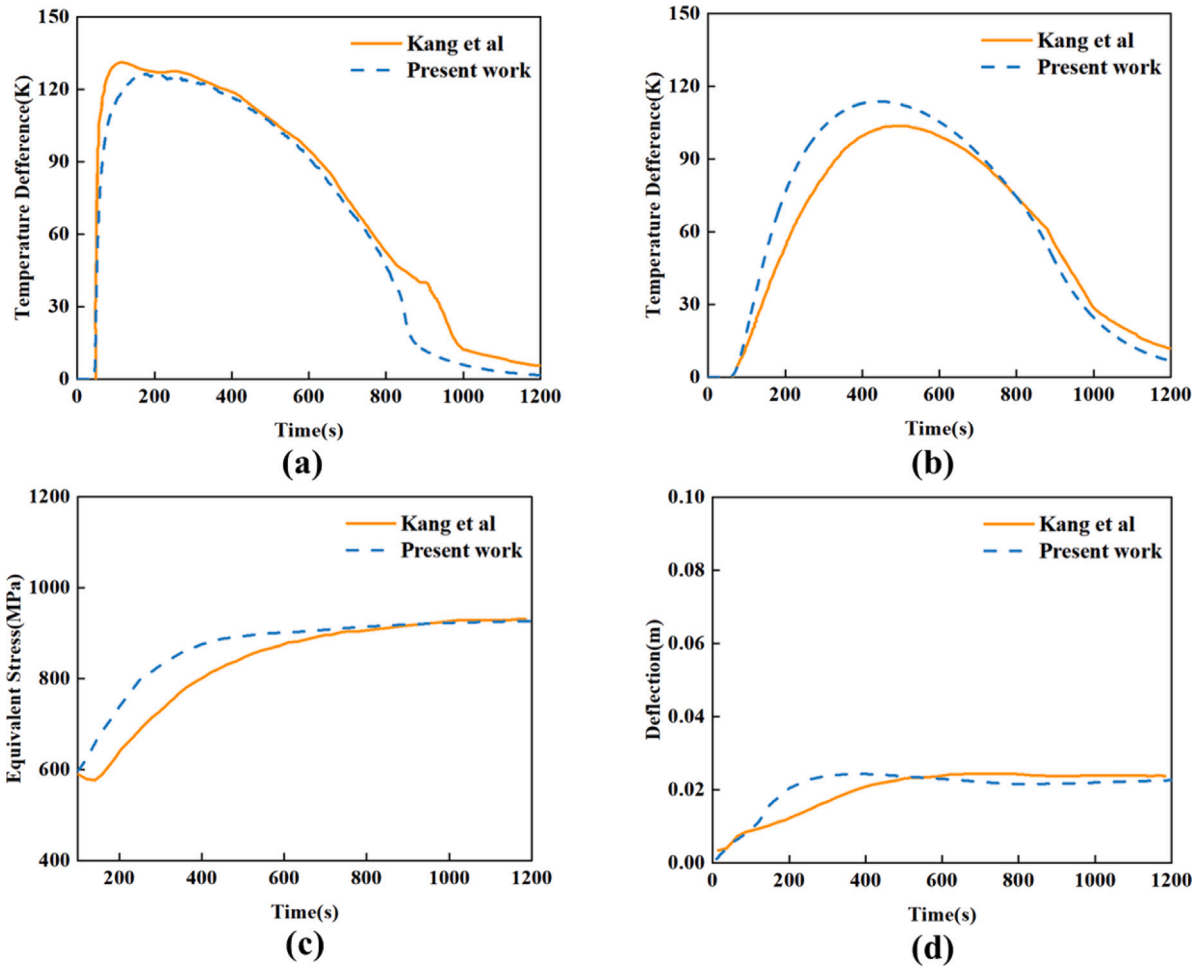

Fig. 3. Validation of the transient conjugate heat transfer simulation as compared to the results reported by Kang et al. (2011) for a pressurizer outsurge. (a) Evolution of temperature difference between the top and bottom inner wall surfaces (Points 1 and 2 in Fig. 1(b)) of section A. (b) Temperature difference between the top and bottom outer wall surfaces (Points 3 and 4 in Fig. 1(b)) of section A. (c) Transient maximum equivalent stress and (d) the maximum deflection.

Table 1
Properties of pipe material and water (Kang et al., 2011).

Parameters	Values
Material of pipe	ASME SA-312 type 316
Density of pipe material ρ_s	8000 kg/m^3
Specific heat capacity of pipe material C_{ps}	500 J/kg K
Conductivity of pipe κ_s	16.3 W/m K
Thermal expansion coefficient of water at 135 °C β_w	9.63×10^{-4}/K
Young's modulus of pipe E	193×10^9 Pa
Poisson's ratio of pipe υ_s	0.3
Thermal expansion coefficient of pipe β_s	17×10^{-6}/K
Velocity of surging flow u	0.07 m/s
Pressurizer water temperature T_H	491.45 K
Heat pipe temperature T_L	324.85 K
Operating pressure P	2.2408 MPa

Table 2
Working condition parameter table.

Parameter	Range
Inner diameter of pressurizer surge line D	200 mm~450 mm
Pressurizer surge line wall thickness δ	16 mm~45 mm
Horizontal pipe section tilt angle θ	0°~15°
Velocity of flow u	0.05 m/s~0.3 m/s
Temperature difference ΔT	10 K~170 K

presents the deflection distribution. Notably, these simulation results align with the findings in the reference paper.

3. Parametric modeling

Thermal stratification is influenced by various factors, including the geometry and arrangement of the surge line, as well as the temperature and velocity of the coolant. To rapidly predict the temperature and stress fields under various operating conditions, we conducted numerous numerical simulations, varying the conditions to establish a comprehensive database. This study incorporates five factors: the inner diameter D, wall thickness δ, the inclination angle θ to the horizontal plane of the surge line, inlet velocity u, and temperature difference ΔT between the cold water from the hot leg and hot water from the pressurizer. The angle of inclination of the horizontal section of the pressurizer surge line plays a crucial role in determining the extent of thermal stratification within the surge line. To accurately model and predict thermal stratification, our methodology incorporates the tilt angle as a variable. By adjusting this angle, we aim to observe and analyze its specific impact on thermal stratification.The tilted arrangement is depicted in Fig. 1(d). Parametric modeling is designed for issues demanding numerous calculation samples. In each sample, only a few key parameters change, while the remaining parameters and calculation settings remain constant. Parametric modeling and calculation eliminate the need for repetitive operations on the GUI interface, enabling automated modeling, calculation, and data collection.

The ranges for the five varying parameters are presented in Table 2. The temperature of the cold fluid is maintained at a constant value of

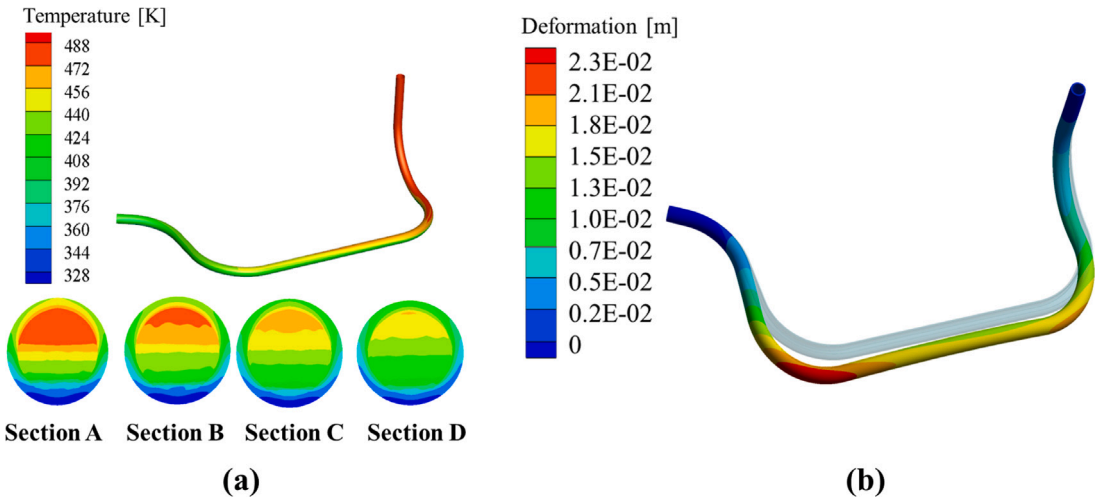

Fig. 4. Thermal stratification of a pressurizer surge line and the induced deflection of the surge line. (a) Temperature distribution at t = 300 s. Temperature contours corresponding to sections marked in Fig. 1(c) are shown. (b) Induced thermal deflection at t = 300 s.

322 K. The Latin hypercube sampling method (Loh, 1996) is employed to extract values for the five parameters in each calculation sample. All calculation settings are specified in batches through Python script, and the varying parameters are cyclically assigned through the journal file of Workbench to perform batch calculations. Ultimately, the entire simulation process is encapsulated in a program that integrates Matlab, journal files, and Python scripts. This program executes steps such as importing the model, meshing, setting boundary conditions, assigning material properties, submitting calculations, post-processing, and saving the results. The integrated procedure is illustrated in Fig. 5. Input variables D, δ, θ refer to the inner diameter, the wall thickness, and the inclination angle of the horizontal part of the surge line, respectively. Variables u and ΔT correspond to the inlet velocity and the temperature difference of the fluid. Totally 100 cases are calculated through parametric modeling and simulation. The acquired temperature fields and thermal stress fields are accumulated as a database.

4. POD-ANN hybrid strategy

Engineering dynamical systems are high-dimensional and deform able nonlinear systems. Processing these high-dimensional systems is prohibitive, particularly due to the time-consuming training and testing processes required for neural networks. Therefore, it is crucial to reduce the degrees of freedom (DOFs) of the system to make it solvable. In this paper, we combine POD and ANN to efficiently predict high-dimensional field information. However, when the geometric parameters of the calculation model change, the number and position of grids also change, making direct mapping impossible. To address this, we introduce a novel POD–ANN hybrid strategy that incorporates the inverse distance weighting (IDW) method and background grids technology, specifically designed to tackle the challenge of predicting in high-dimensional variable geometry systems.

4.1. Background grid and inverse distance weighted (IDW)

The field variables of different cases were collected using the parametric modeling method described earlier. However, the grids of the surge line, with varying geometric parameters, exhibit differences, leading to variations in DOFs. This discrepancy poses an inconvenience for establishing snapshots used in the POD method. To address this, the background grid method (Klok, 1986) and IDW interpolation are employed. These techniques aim to obtain temperature data for an equivalent number of nodes topologically mapped at the fluid–solid interface, as illustrated in Fig. 6. Fig. 6(a) presents the background grids of two surge lines with varying tube diameters and tilt angles. The red grid features a narrower diameter and remains horizontal, while the blue grid exhibits a larger diameter with an inclination. Despite differences in simulation grids, their background grid nodes display a uniform topological distribution. All background grids can be represented in the same two-dimensional unfolded form, containing n nodes. In the present study, we set n = 7728, with 24 nodes uniformly distributed along the β axis and 322 nodes uniformly distributed along the s axis, as depicted in Fig. 6(b). Subsequently, Inverse Distance Weighting (IDW) interpolation was utilized to fill in missing physical information in the background grids. The application of IDW interpolation is demonstrated in Fig. 6(c), facilitating the transfer of the physical field from the simulation grids to the background grids. Specifically, when applying the IDW interpolation method to grid cells at the boundary, the selected sample units should also be the boundary grid cells.

$$\widetilde{T}_i = \frac{\sum_{j=1}^{n} T_j / d_j}{\sum_{j=1}^{n} 1/d_j} \tag{7}$$

where $\widetilde{T}_i$ represents the temperature value on the background grid node i, T_j is the value on the simulation grid node j, d_j is the distance of the nodes. This approach results in equal DOFs at the fluid–solid interfaces across all cases. By employing background grids and the IDW interpolation method, structural parameters or grid quantities are standardized to a common scale. This normalization facilitates more consistent comparisons and analyses across different parameter values.

4.2. Proper orthogonal decomposition (POD)

The initial phase of POD involves constructing a snapshot matrix by combining the database established through the parametric modeling method with the background grid and IDW methods described earlier. Subsequently, we utilize the snapshot-based POD method for model reduction. For an n-DOF system, a snapshot matrix containing m cases (each with 5 input variables) calculated through the parametric modeling method can be constructed as:

$$\mathbf{T}_{snap} = [\mathbf{T}(\mathbf{c}_1) \quad \mathbf{T}(\mathbf{c}_2) \cdots \mathbf{T}(\mathbf{c}_i) \cdots \mathbf{T}(\mathbf{c}_m)] \tag{8}$$

in which m is the total number of simulation cases, $\mathbf{T}(\mathbf{c}_i) = [\widetilde{T}_{1,i} \ \widetilde{T}_{2,i} \cdots \widetilde{T}_{n,i}]^{\mathbf{T}}$ is the temperature field at the fluid–solid interface at a certain moment of ith simulation case, n is the number of background grids. And $\mathbf{c}_i = [D_i \ \delta_i \ \theta_i \ u_i \ \Delta T_i]^{\mathbf{T}}$ is the input variables vector of ith simulation

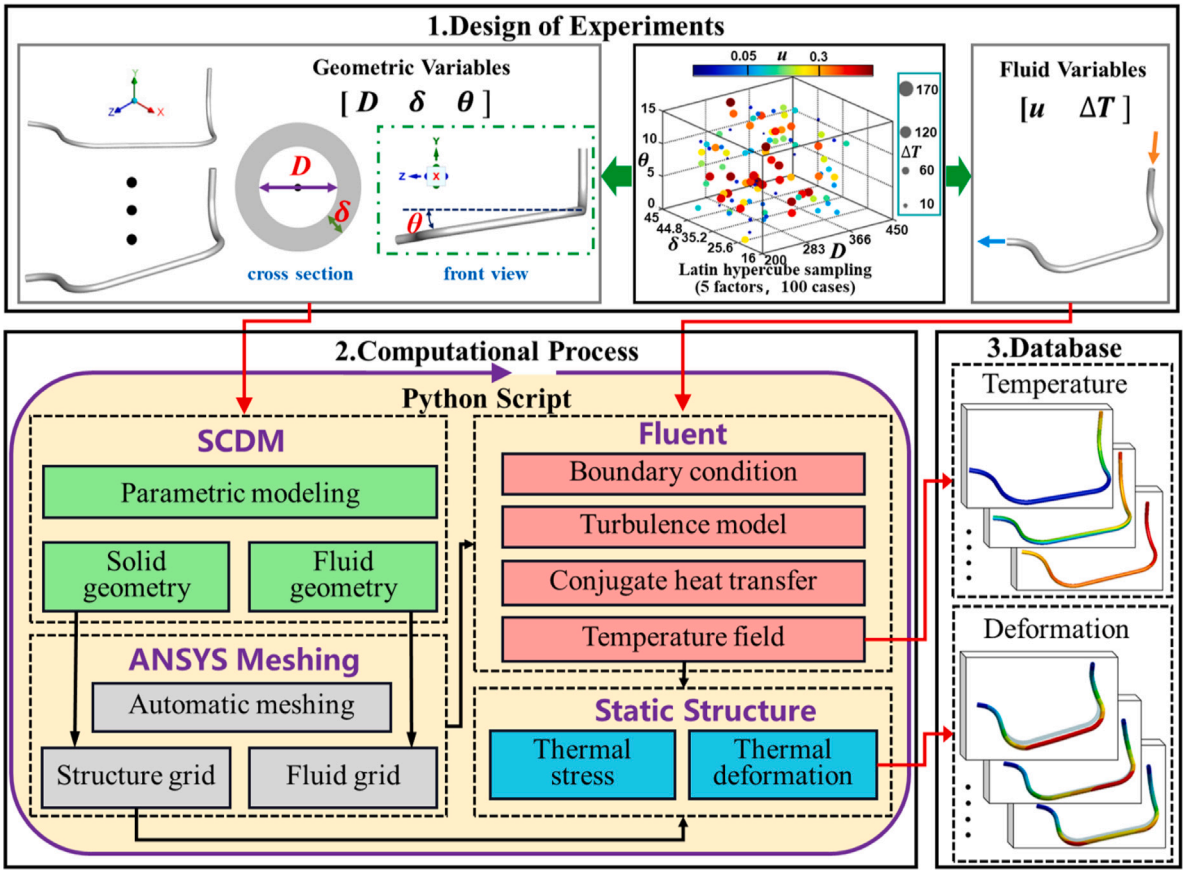

Fig. 5. Flow chart of parametric modeling for conjugate heat transfer in a pressurizer surge line.

case. The singular value decomposition (SVD) is employed in the snapshot matrix.

$$\mathbf{T}_{snap} = \mathbf{\Phi}\mathbf{\Sigma}\mathbf{V}^{*} \tag{9}$$

where $\mathbf{\Phi}$ is the POD mode, $\mathbf{\Sigma}$ is the singular values matrix and $\mathbf{V}$ is the eigenvector matrix. The POD modes $\mathbf{\Phi}$ can be further approximated by a truncated $\bar{\mathbf{\Phi}}$, where $\bar{\mathbf{\Phi}}$ only contains the first l modes. Based on the selection criterion, the first l order POD basis can be selected accordingly:

$$e(l) = \frac{\sum_{j=1}^{l} \lambda_j}{\sum_{j=1}^{m} \lambda_j} \tag{10}$$

where λ_j is the jth entry of the diagonal matrix $\mathbf{\Sigma}$, and $p = min(n, m)$ and $l < p$. Herein, the relative error $\epsilon(l)$ of truncated POD bases is defined as $\epsilon(l) = 1 - e(l)$. The criterion for selecting the minimum l is based on the determination coefficient (R^2) of the prediction results. We keep increasing the order of the truncated POD modes l until the R^2 is larger than 0.99. Consequently, the number of POD modes l for temperature prediction reaches 6, and the l for equivalent stress reaches 10. The relative errors of the truncated POD modes $\epsilon(l)$ are 0.18% and 1% for temperature and equivalent stress prediction, respectively.

Once the truncated POD modes $\bar{\mathbf{\Phi}}$ are obtained, the reduced state vector $\mathbf{q}(\mathbf{c}_i)$ of $\mathbf{T}(\mathbf{c}_i)$ associated with the POD modes are encoding via the following relationship

$$\mathbf{q}(\mathbf{c}_i) = \bar{\mathbf{\Phi}}^{T}\mathbf{T}(\mathbf{c}_i) \tag{11}$$

and, vice versa, for a prediction condition $\hat{\mathbf{c}} = [\hat{D}\ \hat{\delta}\ \hat{\theta}\ \hat{u}\ \hat{\Delta T}]^{\mathbf{T}}$, if $\hat{\mathbf{q}}(\hat{\mathbf{c}})$ is forecasted via artificial neural network (ANN), a full-order data can be decoded as

$$\hat{\mathbf{T}}(\hat{\mathbf{c}}) = \bar{\mathbf{\Phi}}\hat{\mathbf{q}}(\hat{\mathbf{c}}) \tag{12}$$

Following this, the post process software Tecplot was utilized to visualize the temperature field on the fluid–solid interface based on the high-dimensional prediction $\hat{\mathbf{T}}(\hat{\mathbf{c}})$.

4.3. Artificial neural network (ANN)

The architecture of the artificial neural network (ANN) surrogate model is schematically illustrated in the middle of Fig. 7. In this study, a dense, fully connected, feed-forward, 1-hidden-layer ANN was utilized, and the activation produced by the ANN is given as follows:

$$\begin{aligned} \mathbf{z} &= g(\mathbf{w}_1\mathbf{c} + \mathbf{b}_1) \\ \mathbf{q} &= g(\mathbf{w}_2\mathbf{z} + \mathbf{b}_2) \end{aligned} \tag{13}$$

where $\mathbf{w}_1$, $\mathbf{w}_2$ are the weight coefficient matrices, $\mathbf{b}_1$, $\mathbf{b}_2$ are the bias vectors, respectively. The function g is a nonlinear function applied element-wise on its arguments, which is the output from the previous step. $\mathbf{z}$ is the hidden vector, with its scalar components referred to as neurons, and the number of neurons in the hidden layer is 64. Note that $\mathbf{c}$ denotes the input layer with 5 neurons corresponding to $D, \delta, \theta, u, \Delta T$, and $\mathbf{q}$ denotes the output layer with l neurons corresponding to the reduced state vector introduced in Eq. (11). Here, l is the number of the modes in truncated $\bar{\mathbf{\Phi}}$ shown in Eq. (10). g is a nonlinear function applied element-wise on its arguments which is applied to the output from the previous step. Popular choices for g include the logistic function, the hyperbolic tangent function, or the rectified linear unit (or ReLU) function (Tripathy and Bilionis, 2018). In this paper, ReLU was adopted as the activation function in all hidden layers and input layers, and we trained the network using the Adam optimizer.

Once the construction of a surrogate model is completed, it is crucial to evaluate the accuracy of the approximation. The so-called R^2 correlation coefficient is calculated on the test dataset to assess the

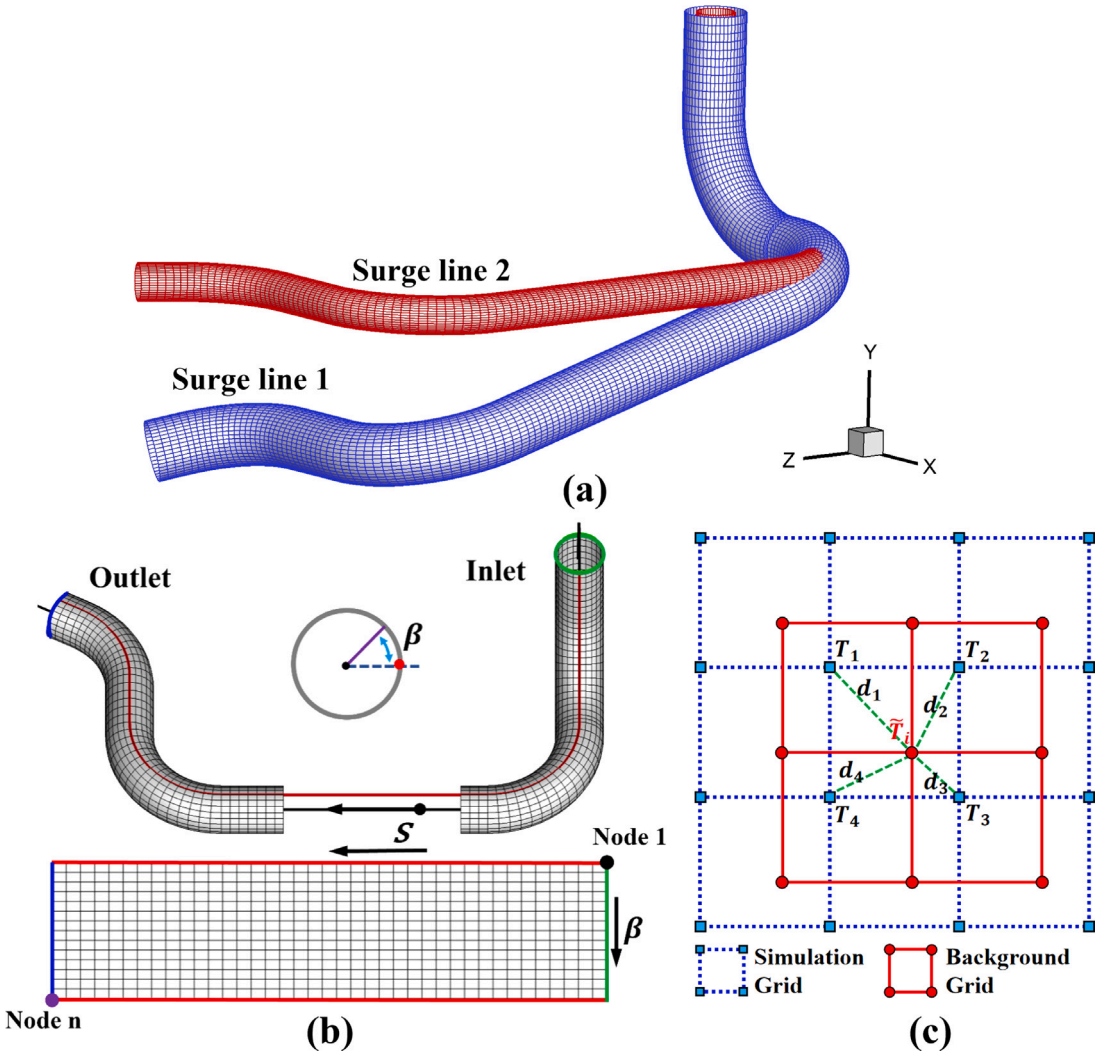

Fig. 6. Background grids generation and illustration of the interpolation method used. (a) Generation of background grids for surge lines with various geometries. (b) The fluid–structure interaction surface grid (top) and its expanded view (bottom) along the central axis are marked in red. (c) Illustration of inverse distance weighted (IDW) interpolation used herein.

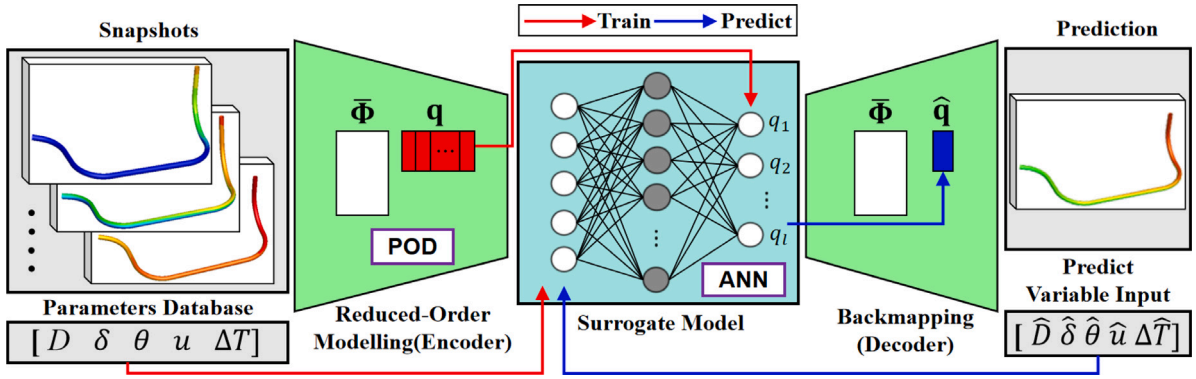

Fig. 7. Schematic of the proposed POD–ANN method.

model's performance. In order to ensure the impact of the number of hidden layer neurons on the model performance in neural network architectures, a sensitivity study is conducted in this paper. In this study, five different configurations were designed for the key parameter of the number of hidden layer neurons: 5 neurons, 10 neurons, 32 neurons, 64 neurons, and 128 neurons. This is shown in the Table 3 below:

As the number of neurons in the hidden layer increases, we observe a gradual improvement in the model's performance on the training set. However, this improvement is not unlimited. When the number of neurons is increased to 128, the enhancement in model performance starts to diminish, and overfitting may even occur, leading to performance degradation on the test set. Therefore, to ensure the accuracy and generalizability of the model, this paper chooses the number of

Table 3
Table of goodness-of-fit for number of neurons.

Number of neurons	R^2
5	0.9952
10	0.9958
32	0.9965
64	0.9969
128	0.9734

neurons to be 64. The surrogate models exhibit excellent performance in terms of temperature and stress fields on the fluid–solid interface, all achieving R^2 measures greater than 98%. The ANN Module in MATLAB was employed for the aforementioned surrogate modeling. Once the surrogate model is established, a predicted reduced state vector $\hat{\mathbf{q}}$ can be obtained using Eq. (13), and the full-order system temperature is decoded by Eq. (12).

4.4. Prediction process

The POD–ANN hybrid approach depicted in Fig. 7 is outlined as follows:

i. Collect input variables matrix of the m simulation cases $\mathbf{C} = [\mathbf{c}_1, \mathbf{c}_2, \ldots, \mathbf{c}_m]$ (each case having 5 variables) and the full-order temperature field data of each cases at a certain moment on fluid–solid interface. And utilize the background grid and IDW methods to establish the snapshot matrix $\mathbf{T}_{snap} = [\mathbf{T}(\mathbf{c}_1), \mathbf{T}(\mathbf{c}_2), \ldots, \mathbf{T}(\mathbf{c}_m)]$.
ii. Afterwards perform POD analysis on $\mathbf{T}_{snap}$ to obtain POD modes $\mathbf{\Phi}$ and the truncated POD modes $\bar{\mathbf{\Phi}}$.
iii. Encode POD reduced state vectors $\mathbf{q}_{snap} = [\mathbf{q}(\mathbf{c}_1), \mathbf{q}(\mathbf{c}_2), \ldots, \mathbf{q}(\mathbf{c}_m)]$ of $\mathbf{T}_{snap}$ through Eq. (11), and then feed $\mathbf{q}_{snap}$ and $\mathbf{C}$ into ANN model as training data.
iv. Obtained the well-trained surrogate model through training by ANN, which establishes a nonlinear mapping between factors and reduced state vector.
v. The ANN surrogate model was used to predict the unknown case's reduced state data $\hat{\mathbf{q}}(\hat{\mathbf{c}})$ under condition $\hat{\mathbf{c}} = [\hat{D}, \hat{\delta}, \hat{\theta}, \hat{u}, \hat{\Delta T}]^{\mathrm{T}}$ by Eq. (13).
vi. Decode a full-order data $\hat{\mathbf{T}}(\hat{\mathbf{c}})$ via Eq. (12).

Ultimately, the post process software Tecplot was employed to visualize the temperature field on the fluid–solid interface based on the high-dimensional prediction $\hat{\mathbf{T}}(\hat{\mathbf{c}})$. The sizes of system variables for the POD–ANN hybrid approach are listed in Table 4: mn

5. Results and discussion

The simulation of surge line thermal stratification was conducted on a PC equipped with an Intel(R) Core(TM) i7-9750H CPU 2.60 GHz processor in the Windows environment. The simulations were carried out for all cases with various parameters, and all calculations were terminated at t = 1000 s. For a single case calculation, using the traditional method can often take up to 17 h, significantly increasing the time cost of the project. When 100 cases need to be processed in batch, the cumulative effect becomes even more significant, totaling over 1700 h, or more than two months of continuous working time. This greatly consumes both time and resources. To overcome this challenge, the innovative hybrid POD–ANN method proposed in this paper significantly improves computational efficiency by combining the advantages of POD and ANN. It takes only 1 min to predict a working condition using the hybrid POD–ANN method. Consequently, processing 100 cases in batch will take just 100 min, drastically reducing the time and cost of calculating working conditions. This efficiency not only enables engineering projects to be completed more quickly but also reduces resource consumption and cost investment in the calculation process.

Each case involved numerous time steps in the transient processing, with thousands of degrees of freedom (DOFs) for temperature information at each time step. Storing and processing such large volumes of time results is impractical. Due to the differences in initial fluid velocities, thermal stratification occurs and fully develops at 600 s in all 100 cases. This time point was chosen as a critical node to explore thermal stratification because, for most cases, it represents a crucial moment. At this time, thermal stratification in the horizontal section of the surge line is prevalent and in a relatively stable state. Prior to this time, the hot water has not yet completely flowed into the surge line, making the thermal stratification phenomenon not yet obvious and accurate prediction and analysis difficult. Conversely, if the selected time point is too late, the water temperature in the surge line has equalized, causing the thermal stratification phenomenon to disappear and rendering the prediction practically insignificant. Therefore, this paper selects 600 s as the key time point for prediction. The temperature data of the fluid–solid coupling surface of the surge line at this moment (t = 600 s) in all cases are summarized to form a snapshot matrix. Although only the 600 s moment is predicted in this paper, it does not imply that the thermal stratification and thermal stress conditions at other moments are unimportant. On the contrary, future studies can further extend the time range to reveal more comprehensively the thermal behavior characteristics of the surge line at different time points.

After completing 100 sets of numerical simulations and batch post-processing, the snapshot matrix of all simulated cases was finally constructed. Singular value decomposition (SVD) was then performed on the snapshot matrix, yielding the corresponding POD modes. Fig. 8 illustrates the six leading POD modes of surge line temperature distribution. These POD modes, denoted as $\mathbf{\Phi}$, were projected onto a certain surge line fluid–solid interface geometry. The red frames in Fig. 8 represent the bottom view of each POD mode. Fig. 8(a) captures the characteristic where the thermal amplitude of the upstream is larger than the thermal amplitude of the downstream, consistent with the physical phenomenon of hot water flowing from the inlet to the outlet. Fig. 8(c) illustrates that mode 3 captures the thermal stratification of the surge line. Once the POD modes were obtained, the ANN method was employed to build the surrogate model between the initial five parameters and the POD state coefficients.

Fig. 9 exhibits the temperature distribution on fluid–structure interaction surface for two predicted cases. For case A the five variables get the values as follows: $\hat{r}$ = 169.9 mm, $\hat{\delta}$ = 38.6 mm, $\hat{\theta}$ = 8.4°, $\hat{u}$ = 0.0798 m/s, $\Delta\hat{T}$ = 52.2 K and for case B $\hat{r}$ = 208.5 mm, $\hat{\delta}$ = 17.9 mm, $\hat{\theta}$ = 1.2°, $\hat{u}$ = 0.0994 m/s, $\Delta\hat{T}$ = 62.7 K. The POD–ANN predictions align well with the CFD results as shown in Fig. 9. The flow and thermal fields in the surge line are highly complex, involving the mixing of two fluids with different temperatures. Additionally, simultaneous convection heat transfer between the surging water and the wet wall, along with heat conduction through the pipe wall, further contribute to the complexity. In Fig. 9(a) and (b), the transient temperature distribution on the wet wall surface is depicted. It illustrates that hot water flows into the surge line from the nozzle at the bottom of the pressurizer. The vertical section of the surge line warms up rapidly, indicating a clear thermal stratification in the horizontal section. To quantify the quality of temperature predictions, we used the coefficient of determination (R_T^2) over all spatial locations which is defined in Eq. (14). R_T^2 is usually between zero to one,

$$R_T^2 = 1 - \frac{\sum_{i=1}^{n}(T_i - \hat{T}_i)^2}{\sum_{i=1}^{n}(T_i - \bar{T}_i)^2} \tag{14}$$

where T_i is the CFD temperature data, $\hat{T}_i$ represents the predicted temperature data, and $\bar{T}_i$ is the mean of the CFD temperature data. In addition, n is the DOFs on the fluid–structure interaction surface.The R_T^2 values for case A and case B are 0.9983 and 0.9876, respectively,

Table 4
System variables and matrix size of POD–ANN method.

System variables	Size
Snapshot matrix $\mathbf{T}_{snap}$	$n \times m$ (n-number of DOFs, m-number of simulation cases)
POD modes $\mathbf{\Phi}$	$n \times m$
Truncated POD modes $\bar{\mathbf{\Phi}}$	$n \times l$ (l-number of truncated POD modes)
Reduced snap matrix $\mathbf{q}_{snap}$	$l \times m$
ANN input $\mathbf{c}$	5 (number of simulation parameters $[D, \delta, \theta, u, \Delta T]$)
ANN output $\mathbf{q}$	l (number of POD state coefficients)

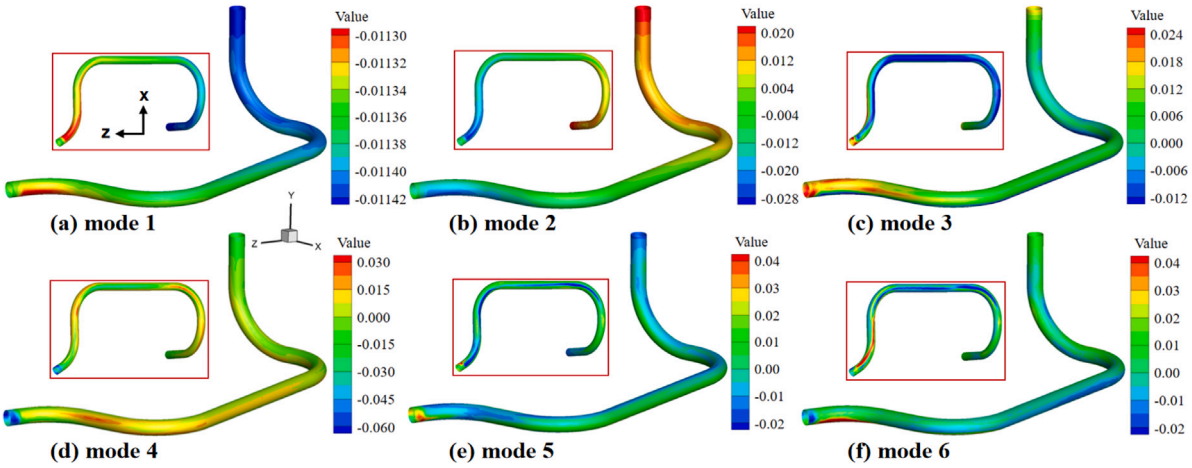

Fig. 8. Calculated six leading POD modes of surge line temperature distribution.

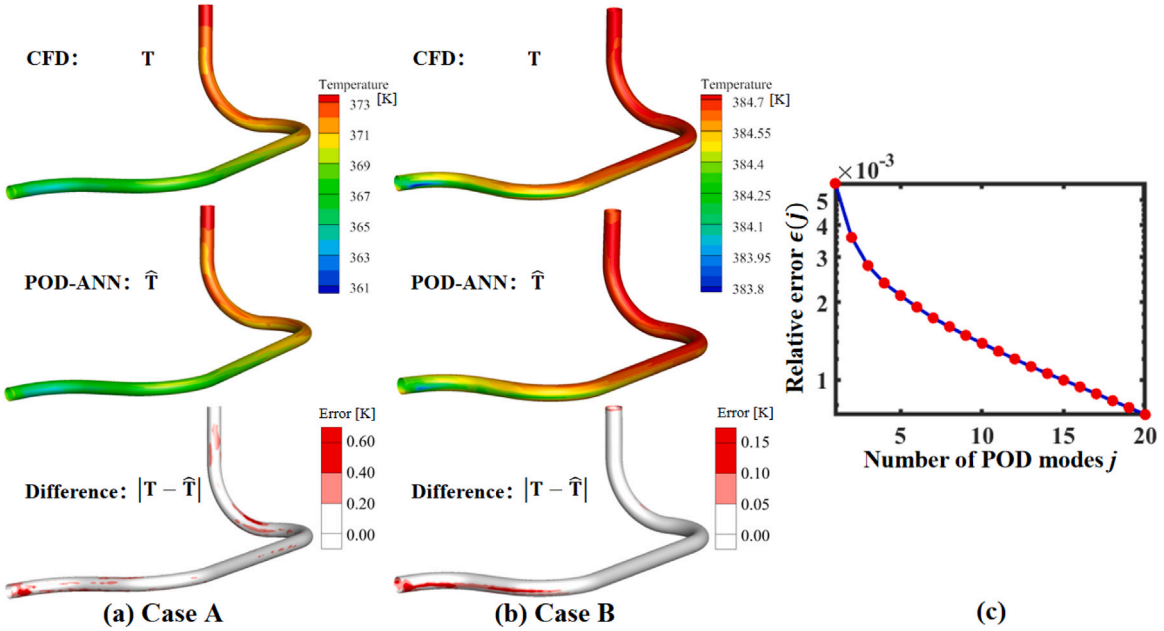

Fig. 9. Digital twins for surge line temperature distribution are depicted in (a) and (b), showcasing comparisons between ground truth CFD simulations of interfacial temperature and their digital twins obtained via POD–ANN, alongside relative error distribution for case A ($\hat{r}$ = 169.9 mm, $\hat{\delta}$ = 38.6 mm, $\hat{\theta}$ = 8.4°, $\hat{u}$ = 0.0798 m/s, $\Delta\hat{T}$ = 52.2 K) and case B ($\hat{r}$ = 208.5 mm, $\hat{\delta}$ = 17.9 mm, $\hat{\theta}$ = 1.2°, $\hat{u}$ = 0.0994 m/s, $\Delta\hat{T}$ = 62.7 K). Additionally, (c) shows the number of POD modes used and the associated relative truncated error for the temperature field.

reaffirming the accuracy of digital twins obtained via POD–ANN. Furthermore, to explore the differential distribution on the surge line internal face for cases A and B, the error cloud plots are mapped by absolute error $|\mathbf{T} - \hat{\mathbf{T}}|$, as shown in the bottom of Fig. 9(a) and (b). The absolute error of both cases is less than 0.7 K, demonstrating the feasibility of the POD–ANN hybrid method. The absolute error of the horizontal tube section is very close to 0 (white in the error contour), indicating that the digital twins of the temperature field can effectively capture the phenomenon of thermal stratification in the horizontal section. The optimal number of truncated POD modes is determined by plotting the relative error $\epsilon(l)$ as a function of the number of POD modes l, as shown in Fig. 9(c). It can be observed that the relative error function goes down with increasing the number of POD modes, and when the number reaches 6, the relative error of the truncated POD modes is below 0.18%. Hence, 6 POD modes are chosen and then used to predict temperature distribution on fluid–structure interaction surface.

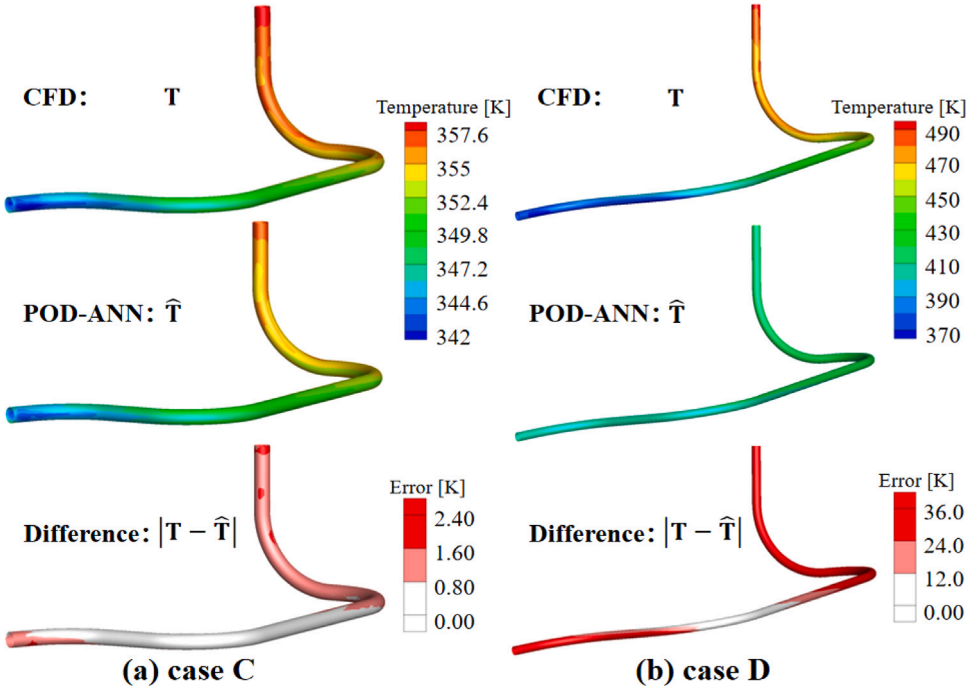

Fig. 10. Accuracy assessment of digital twins for surge line temperature distribution under parameters outside the initial range are depicted in (a) and (b). These plots illustrate a comparison between the ground truth CFD simulation of interfacial temperature and its digital twins obtained via POD–ANN, alongside relative error distribution for case C ($\hat{r}$ = 158.1 mm, $\hat{\delta}$ = 42.4 mm, $\hat{\theta}$ = 0.56°, $\hat{u}$ = 0.045 m/s, $\Delta\hat{T}$ = 36.9 K) and case D ($\hat{r}$ = 90 mm, $\hat{\delta}$ = 65 mm, $\hat{\theta}$ = 16°, $\hat{u}$ = 0.04 m/s, $\Delta\hat{T}$ = 180 K), respectively.

To further explore the application of the POD–ANN method in the numerical simulation of thermal stratification in surge lines, we predicted the temperature distribution on the fluid–structure interaction surface in two cases where variables were selected outside the range of the five initial simulation parameters. Fig. 10 illustrates the CFD results, predicted results, and error distribution for both cases. In case C, the values of the five variables are as follows: $\hat{r}$ = 158.1 mm, $\hat{\delta}$ = 42.4 mm, $\hat{\theta}$ = 0.56°, $\hat{u}$ = 0.045 m/s, $\Delta\hat{T}$ = 36.9 K, with the flow velocity parameter falling below the working condition range. The R_T^2 value of the temperature distribution on the fluid–structure interaction surface is 0.958, indicating strong alignment between the POD–ANN predictions and the CFD results. The discrepancy between the CFD result and the POD–ANN prediction is depicted at the bottom of Fig. 10(a), with an absolute error of less than 3 K. This demonstrates that the POD–ANN hybrid method remains viable even when the parameters extend beyond the initial sample range. In the case of D, with $\hat{r}$ = 90 mm, $\hat{\delta}$ = 65 mm, $\hat{\theta}$ = 16°, $\hat{u}$ = 0.04 m/s, $\Delta\hat{T}$ = 180 K, all five working condition parameters are outside the range of the initial set values. The POD–ANN prediction results significantly differ from those of the CFD, with an R_T^2 value of temperature distribution on the fluid–structure interaction surface of −0.135. The absolute error between the CFD result and the POD–ANN prediction, shown at the bottom of Fig. 10(b), indicates that most areas on the fluid–structure interaction surface exhibit differences higher than 12 K. Further research is required to determine the feasibility and applicability of each parameter beyond the initial range in the POD–ANN method.

The accuracy of digital twins for surge line equivalent stress distribution is also evaluated, as depicted in Fig. 11. The equivalent stress distribution on the fluid–structure interaction surface for two predicted cases. In case A, the values for the five variables are $\hat{r}$ = 169.9 mm, $\hat{\delta}$ = 38.6 mm, $\hat{\theta}$ = 8.4°, $\hat{u}$ = 0.0798 m/s, and $\Delta\hat{T}$ = 52.2 K. For case B, the values are $\hat{r}$ = 208.5 mm, $\hat{\delta}$ = 17.9 mm, $\hat{\theta}$ = 1.2°, $\hat{u}$ = 0.0994 m/s, and $\Delta\hat{T}$ = 62.7 K. To quantify the quality of stress distribution predictions, we used the coefficient of determination (R_S^2) over all spatial locations which is defined in Eq. (15). R_S^2 is usually between zero to one,

$$R_S^2 = 1 - \frac{\sum_{i=1}^{n}(S_i - \hat{S}_i)^2}{\sum_{i=1}^{n}(S_i - \bar{S}_i)^2} \tag{15}$$

where S_i is the FEM stress distribution, $\hat{S}_i$ represents the predicted stress distribution, and $\bar{S}_i$ is the mean of the FEM stress distribution. In addition, n is the DOFs on the fluid–structure interaction surface. The R_S^2 values for case A and case B are 0.9765 and 0.9903, respectively, indicating that the predictions from POD–ANN are also in good agreement with the finite element simulation results. The transient distributions of equivalent forces in the pressurizer surge line for the two operating conditions are depicted in Fig. 11(a) and (b), with the maximum equivalent forces located at both ends of the pressurizer surge line. The error cloud plots of equivalent stress distribution on the surge line internal face for each case were shown at the bottom of Fig. 11(a) and (b), In case A, the larger error distribution is observed in the downstream segment, whereas for case B, the larger error distribution is at the ends of the pressurizer surge line. Given that the maximum stress value is approximately 3.8×10^8 Pa and the absolute error is 8×10^6 Pa, it can be inferred that numerical twinning can effectively reconstruct not only the temperature variable but also the stress variable. Meanwhile, with the number of POD modes reaching 10, the relative error of the truncated POD modes remains below 1%, as illustrated in Fig. 11(c). 10 POD modes are selected and utilized to predict the distribution of equivalent stress on the fluid–structure interaction surface.

Despite the accurate predictions, the computational time required for POD–ANN is negligible compared to conventional simulations. This enables real-time predictions of thermal stratification under any working condition.

6. Conclusion

Piping systems are extensively adopted in power plants. A long horizontal pipe is susceptible to thermal stratification if a hot fluid and a cold fluid meet and mix in the pipe. A pressurizer surge line belongs to this type of line, and several incidents of thermal stratification of surge lines have been reported and have drawn great safety concerns. Thermal stratification of a pressurizer surge line is affected by a number of geometric and physical parameters. It is highly desirable to assess the thermal and structural behaviors of the surge line under thermal

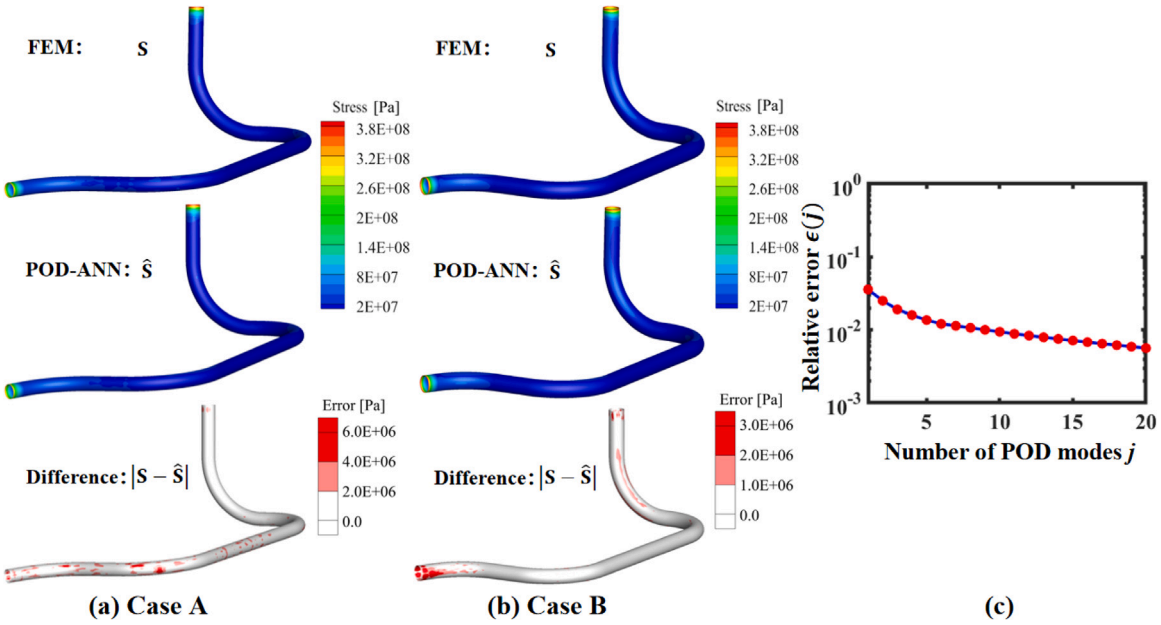

Fig. 11. Digital twins for surge line equivalent stress distribution are illustrated in (a) and (b), displaying comparisons between ground truth CFD simulations of interfacial stress and their digital twins obtained via POD–ANN, accompanied by relative error distribution for case A and B, respectively. Additionally, (c) presents the number of POD modes used and the associated relative truncated error for stress.

stratification conditions, covering all possible parameter variations of interest. The assessment should be carried out in an in-line, real-time way and should be completed as quickly as possible, which calls for the construction of digital twins of surge lines subjected to thermal stratification loadings as virtual replicas of real physical systems. Complicated one-way coupled conjugate heat transfer is involved in the thermal stratification and thermal stress analysis of surge lines, which entails high-quality meshing generation and high cost CFD and FEM simulations. Constructing digital twins of such a multiphysics coupling problem necessitates access to a host of a forbidden task if high-fidelity simulations are used exclusively.

This paper describes a hybrid POD–ANN approach to construct a surrogate-assisted digital twining of a surge line subjected to thermal stratification. A parametric modeling of the conjugate heat transfer problem was performed. In exploring the thermal stratification phenomenon, this paper has identified 600 s as a critical time point. At this certain moment, the thermal stratification phenomenon within the horizontal section of the surge line is not only prevalent but also exhibits a relatively stable state, providing ideal conditions to study its properties and mechanisms. Therefore, at this specific moment, special attention was given to field variables such as temperature and stress on the fluid–structure interaction surface. These critical data were comprehensively collected and meticulously stored for subsequent analysis. Possible parameter variations were also considered to ensure the data's comprehensiveness and accuracy. And an inverse distance weighted (IDW) interpolation method was introduced to generate a background grid with fixed topology regardless of variations of surge line geometries, which facilitates the collection of simulation data on a fixed grid and the construction of the snapshot matrix for reduced-order modeling. Subsequently, the popular proper orthogonal decomposition (POD) technology was used here based on the snapshot matrix, and the reduced state coefficients were obtained. A surrogate model was then established by using ANN, and a relationship between the design parameters of the surge line and the reduced state coefficients of POD modes was built in a black-box way. Here, the inner diameter D, the wall thickness δ, the inclination angle θ, the inlet velocity u and the temperature difference ΔT of the surge line were chosen as design variables for demonstration, and a three-layers ANN for data regression, resulting in a feasible and flexible numerical strategy for digital twinning. Finally, we introduce a novel POD–ANN hybrid strategy that incorporates the background grids and IDW method, specifically designed to tackle the challenge of predicting in high-dimensional variable geometry nuclear systems. In summary, we proposed a novel POD–ANN hybrid strategy that incorporates the background grids and the IDW method, specifically designed to tackle the challenge of predicting high-dimensional variable geometry nuclear systems. The precision of digital twins established by POD–ANN approach for surge line temperature and thermal stress distribution was ensured by monitoring the determination coefficient (R^2) and the relative error cloud plots. Some preliminary study on the performance of the current method for parameter extrapolation was also carried out, and the method demonstrates a limited extrapolation capability. Nevertheless, the improvement of the approach for better extrapolation performance under large parameter variation remains an open question for future study. The proposed approach has been implemented in commercial software through scripting, and the codes are accessible via the provided link. The accessibility of the codes and the compatibility with commercial software would facilitate broad application in the community, given the fact that the study on surrogate-assisted digital twins is fairly limited in the literature for such a complex thermo–fluid–structure interaction problem.

CRediT authorship contribution statement

Ying Yang: Writing – original draft, Validation, Software, Data curation, Conceptualization. **Xielin Zhao:** Writing – original draft, Software, Methodology, Formal analysis, Conceptualization. **Qian Cheng:** Visualization, Validation, Investigation. **Ruiwen Guo:** Investigation, Formal analysis. **Meie Li:** Writing – original draft, Validation, Software, Investigation, Conceptualization. **Jinxiong Zhou:** Writing – original draft, Project administration, Funding acquisition.

Declaration of competing interest

The authors declare that they have no known competing financial interests or personal relationships that could have appeared to influence the work reported in this paper.

Data availability

The raw/processed data required to reproduce these findings are available to download from [https://github.com/XJTU-Zhou-group/DigitalTwin].

Acknowledgments

This research is supported by the National Natural Science Foundation of China (grant 11972277) and by Science Technology on Reactor System Design Technology Laboratory, China (LRSDT2021205).

References

Baiges, J., Codina, R., Castanar, I., Castillo, E., 2020. A finite element reduced-order model based on adaptive mesh refinement and artificial neural networks. Int. J. Numer. Methods Eng. 121, 588–601.
Blanc, T.J., Jones, M.R., Gorrell, S.E., 2016. Reduced-order modeling of conjugate heat transfer processes. J. Transf. 138, 051703.
Cai, B., Weng, Y., Wang, Y., Qin, X., Cao, F., Gu, H., Wang, H., 2017. Experimental investigation on thermal stratification in a pressurizer surge line with different arrangements. Prog. Nucl. Energy 98, 239–247.
Do Kweon, H., Kim, J.S., Lee, K.Y., 2008. Fatigue design of nuclear class 1 piping considering thermal stratification. Nucl. Eng. Des. 238, 1265–1274.
Eftekhar Azam, S., Rageh, A., Linzell, D., 2019. Damage detection in structural systems utilizing artificial neural networks and proper orthogonal decomposition. Struct. Control Health Monit. 26, e2288.
Fresca, S., Manzoni, A., 2022. POD-DL-ROM: Enhancing deep learning-based reduced order models for nonlinear parametrized PDEs by proper orthogonal decomposition. Comput. Methods Appl. Mech. Eng. 388, 114181.
Fuller, A., Fan, Z., Day, C., Barlow, C., 2020. Digital twin: Enabling technologies, challenges and open research. IEEE Access 8, 108952–108971.
Grieves, M.W., 2005. Product lifecycle management: the new paradigm for enterprises. Int. J. Prod. Dev. 2, 71–84.
He, S., Wang, M., Zhang, J., Tian, W., Qiu, S., Su, G., 2022. A deep-learning reduced-order model for thermal hydraulic characteristics rapid estimation of steam generators. Int. J. Heat Mass Transf. 198, 123424.
Hu, L.-W., Kazimi, M.S., 2006. LES benchmark study of high cycle temperature fluctuations caused by thermal striping in a mixing tee. Int. J. Heat Fluid Flow 27, 54–64.
Im, S., Lee, J., Cho, M., 2021. Surrogate modeling of elasto-plastic problems via long short-term memory neural networks and proper orthogonal decomposition. Comput. Methods Appl. Mech. Eng. 385, 114030.
Jo, J.C., Kang, D.G., 2010. CFD analysis of thermally stratified flow and conjugate heat transfer in a PWR pressurizer surgeline. J. Press. Vessel Technol. 132.
Jones, D., Snider, C., Nassehi, A., Yon, J., Hicks, B., 2020. Characterising the digital twin: A systematic literature review. CIRP J. Manuf. Sci. Technol. 29, 36–52.
Kamaya, M., 2014. Assessment of thermal fatigue damage caused by local fluid temperature fluctuation (part I: characteristics of constraint and stress caused by thermal striation and stratification). Nucl. Eng. Des. 268, 121–138.
Kamaya, M., Nakamura, A., 2011. Thermal stress analysis for fatigue damage evaluation at a mixing tee. Nucl. Eng. Des. 241, 2674–2687.
Kang, D.G., Jhung, M.J., Chang, S.H., 2011. Fluid–structure interaction analysis for pressurizer surge line subjected to thermal stratification. Nucl. Eng. Des. 241, 257–269.
Kim, S.-H., Choi, J.-B., Park, J.-S., Choi, Y.-H., Lee, J.-H., 2013. A coupled CFD-FEM analysis on the safety injection piping subjected to thermal stratification. Nucl. Eng. Des. 45, 237–248.
Kim, S.-N., Hwang, S.-H., Yoon, K.-H., 2005. Experiments on the thermal stratification in the branch of NPP. J. Mech. Sci. Technol. 19, 1206–1215.
Kim, J., Roidt, R., Deardorff, A., 1993. Thermal stratification and reactor piping integrity. Nucl. Eng. Des. 139, 83–95.
Klok, F., 1986. Two moving coordinate frames for sweeping along a 3D trajectory. Comput. Aided Geom. Design 3 (3), 217–229.
Kritzinger, W., Karner, M., Traar, G., Henjes, J., Sihn, W., 2018. Digital twin in manufacturing: A categorical literature review and classification. Ifac-PapersOnline 51, 1016–1022.
Lee, J.I., Hu, L.-w., Saha, P., Kazimi, M.S., 2009. Numerical analysis of thermal striping induced high cycle thermal fatigue in a mixing tee. Nucl. Eng. Des. 239, 833–839.
Liu, T., Cranford, E., 1991. An investigation of thermal stress ranges under stratification loadings. J. Press. Vessel Technol. 113, 326–331.
Liu, T., Zhao, X., Sun, P., Zhou, J., 2024. A hybrid proper orthogonal decomposition and next generation reservoir computing approach for high-dimensional chaotic prediction: Application to flow-induced vibration of tube bundles. Chaos 34 (3).
Loh, W.-L., 1996. On latin hypercube sampling. Ann. Stat. 24 (5), 2058–2080.
Miksch, M., Lenz, E., Löhberg, R., 1985. Loading conditions in horizontal feedwater pipes of LWRs influenced by thermal shock and thermal stratification effects. Nucl. Eng. Des. 84, 179–187.
Muhammad, N., Wang, M., Tian, W., Su, G., Qiu, S., 2022. LES study on the turbulent thermal stratification and thermo-mechanical fatigue analysis for NPP surge line. Int. J. Therm. Sci. 178, 107608.
Park, K.H., Jun, S.O., Baek, S.M., Cho, M.H., Yee, K.J., Lee, D.H., 2013. Reduced-order model with an artificial neural network for aerostructural design optimization. J. Aircr. 50, 1106–1116.
Pawar, S., Rahman, S.M., Vaddireddy, H., San, O., Rasheed, A., Vedula, P., 2019. A deep learning enabler for nonintrusive reduced order modeling of fluid flows. Phys. Fluids 31.
Pearson, K., 1901. LIII. On lines and planes of closest fit to systems of points in space. Lond. Edinb. Dublin Philos. Mag. J. Sci. 2 (11), 559–572.
Qiao, S., Gu, H., Wang, H., Luo, Y., Wang, D., Liu, P., Wang, Q., Mao, Q., 2014. Experimental investigation of thermal stratification in a pressurizer surge line. Ann. Nucl. Energy 73, 211–217.
San, O., Maulik, R., Ahmed, M., 2019. An artificial neural network framework for reduced order modeling of transient flows. Commun. Nonlinear Sci. Numer. Simul. 77, 271–287.
Shah, N.V., Girfoglio, M., Quintela, P., Rozza, G., Lengomin, A., Ballarin, F., Barral, P., 2022. Finite element based model order reduction for parametrized one-way coupled steady state linear thermo-mechanical problems. Finite Elem. Anal. Des. 212, 103837.
Talja, A., Hansjosten, E., 1990. Results of thermal stratification tests in a horizontal pipe line at the HDR-facility. Nucl. Eng. Des. 118, 29–41.
Tao, F., Qi, Q., 2019. Make more digital twins. Nature 573 (7775), 490–491.
Tao, F., Zhang, H., Liu, A., Nee, A.Y., 2018. Digital twin in industry: State-of-the-art. IEEE Trans. Ind. inform. 15 (4), 2405–2415.
Tian, W., Wei, J., Wang, Z., Su, G., Qiu, S., 2017. Experimental investigation on flooding of AP1000 pressurizer surge line. Nucl. Power Eng. 38 (5), 151–155.
Tripathy, R.K., Bilionis, I., 2018. Deep UQ: Learning deep neural network surrogate models for high dimensional uncertainty quantification. J. Comput. Phys. 375, 565–588.
Wang, M., Feng, T., Fang, D., Hou, T., Tian, W., Su, G., Qiu, S., 2019. Numerical study on the thermal stratification characteristics of AP1000 pressurizer surge line. Ann. Nucl. Energy 130, 8–19.
Wright, L., Davidson, S., 2020. How to tell the difference between a model and a digital twin. Adv. Model. Simul. Eng. Sci. 7, 1–13.
Yu, H., Li, L., Tang, Q., Peng, Y., Li, Y., 2022. Transient behaviors of thermo-hydraulic and thermal stratification in the pressurizer surgeline for the nuclear power plant. J. Therm. Sci. 31, 344–358.
Yu, Y., Park, S., Sohn, G., Bak, W., 1997. Structural evaluation of thermal stratification for PWR surge line. Nucl. Eng. Des. 178, 211–220.
Zhao, X., An, N., Yang, G., Wang, J., Tang, H., Li, M., Zhou, J., 2021. Enhancing standard finite element codes with POD for reduced order thermal analysis: Application to electron beam melting of pure tungsten. Mater. Today Commun. 29, 102796.
Zhao, X., Cheng, Q., Yu, X., Huang, Q., Zhang, K., Feng, Z., Zhou, J., 2023. Modal analysis of lead-bismuth eutectic flow in a single wire-wrapped rod channel. Ann. Nucl. Energy 191, 109918.